Journal of Materials Chemistry A

PAPER

View Article Online
View Journal | View Issue

Open Access Article. Published on 20 April 2015. Downloaded on 7/22/2025 6:37:52 AM.
This article is licensed under a Creative Commons Attribution 3.0 Unported Licence.

Cite this: J. Mater. Chem. A, 2015, 3, 11985

Improved oxide-ion conductivity of $NdBaInO_4$ by Sr doping†

Kotaro Fujii,[a] Masahiro Shiraiwa,[a] Yuichi Esaki,[b] Masatomo Yashima,*[a] Su Jae Kim[c] and Seongsu Lee[c]

Received 18th February 2015
Accepted 12th April 2015

DOI: 10.1039/c5ta01336d

www.rsc.org/MaterialsA

The oxide-ion conductivity of $NdBaInO_4$ has been increased by Sr doping. $Nd_{0.9}Sr_{0.1}BaInO_{3.95}$ showed the highest electrical conductivity among $Nd_{1-x}Sr_xBaInO_{4-x/2}$ (x = 0.0, 0.1, 0.2, and 0.3). The oxide-ion conductivity σ_{ion} of $Nd_{0.9}Sr_{0.1}BaInO_{3.95}$ ($\sigma_{ion} = 7.7 \times 10^{-4}$ S cm^{-1}) is about 20 times higher than that of $NdBaInO_4$ ($\sigma_{ion} = 3.6 \times 10^{-5}$ S cm^{-1}) at 858 °C, and the activation energy of oxide-ion conduction is a little lower for $Nd_{0.9}Sr_{0.1}BaInO_{3.95}$ (0.795(10) eV) than that for $NdBaInO_4$ (0.91(4) eV). The structure analysis based on neutron powder diffraction data revealed that the Sr exists at the Nd site and oxygen vacancies are observed in $Nd_{0.9}Sr_{0.1}BaInO_{3.95}$. This result indicates that the increase of the oxide-ion conductivity is mainly due to the increase of the carrier concentration. The bond valence-based energy landscape indicated two-dimensional oxide-ion diffusion in the $(Nd,Sr)_2O_3$ unit on the bc-plane and a decrease of the energy barrier by the substitution of Nd with Sr cations.

Introduction

Oxide-ion conductors, which include pure ionic conductors and mixed oxide-ion and electronic conductors, attract significant interest because of their varied uses in oxygen separation membranes and cathodes for solid-oxide fuel cells (SOFCs).[1] The oxide-ion conductivity is strongly dependent on the crystal structure and particularly the defects. At present, several structures, such as fluorites,[2,3] perovskites,[2,4] K_2NiF_4,[2,5] mellilites,[2,6] and apatites,[2,7] are known to show high oxide-ion conductivities. Further development of oxide-ion conductors involves investigating materials with new types of structures. Recently, we have discovered a new structure family of oxide-ion conductors based on $NdBaInO_4$, a monoclinic $P2_1/c$ perovskite-related phase with a layered structure.[8] In this study, we have successfully improved the oxide-ion conductivity of $NdBaInO_4$ by Sr doping at the Nd site, which aims to increase the concentration of oxygen vacancies (*i.e.*, carriers for the oxide-ion conduction) and to lower the activation energy by exchanging Nd^{3+} with the larger Sr^{2+} cation. This study reports on the electrical conductivity and the crystal structure of Sr-doped $NdBaInO_4$. The electrical conductivity of $NdBaInO_4$ was also investigated again for comparison.

Experimental section

Synthesis and characterization of the chemical composition

$Nd_{1-x}Sr_xBaInO_{4-x/2}$ (x = 0.0, 0.1, 0.2, 0.3, and 0.4) compounds were synthesized by solid-state reactions. Nd_2O_3 (99.95% purity) and $BaCO_3$ (99.9% purity) from Kanto Chemical Co. Inc., $SrCO_3$ and In_2O_3 (both 99.9% purity) from Kojundo Chemical Lab. Co., Ltd. were accurately weighed in $1-x : 1 : x : 1$ cation molar ratios, and they were mixed and ground using a planetary ball mill (Fritsch, P7) for 30 min. The mixtures were calcined at 1000 °C for 8 h in air for decarbonization. Then, the calcined mixtures were milled again for 30 min and uniaxially pressed into pellets at about 50 MPa. These pellets were sintered in air at 1400 °C for 24 h.

The cation ratio of $Nd_{0.9}Sr_{0.1}BaInO_{3.95}$ was confirmed by inductively coupled plasma optical emission spectrometry (ICP-OES) as Nd : Sr : Ba : In = 0.919(8) : 0.0996(9) : 0.992(3) : 0.989(9), which agreed with the average chemical composition of the starting mixture, Nd : Sr : Ba : In = 0.9 : 0.1 : 1 : 1 within 3σ. Here, the σ is the standard deviation of the measured chemical composition and the number in the parenthesis is the last digit of σ.

Thermogravimetric analyses (TGA) of $NdBaInO_4$ and $Nd_{0.9}Sr_{0.1}BaInO_{3.95}$ in Ar flow (50 mL min^{-1}) were conducted using a Bruker-AXS TG-DTA2020SA instrument with heating and cooling rates of 10 °C min^{-1}. The TG measurements were repeated three times to confirm the reproducibility and minimize artefacts from adsorbed species such as water.

[a]Department of Chemistry and Materials Science, Graduate School of Science and Engineering, Tokyo Institute of Technology, 2-12-1-W4-17, O-okayama, Meguro-ku, Tokyo 152-8551, Japan

[b]Department of Chemistry, Graduate School of Science and Engineering, Tokyo Institute of Technology, 2-12-1-W4-17, O-okayama, Meguro-ku, Tokyo 152-8551, Japan

[c]Neutron Science Division, Research Reactor Utilization Department, Korea Atomic Energy Research Institute, 1045 Daedeok-daero, Yuseong-gu, Daejeon, 305-353, Korea

† Electronic supplementary information (ESI) available: A document containing the crystallographic data of $Nd_{0.9}Sr_{0.1}BaInO_{3.95}$, additional experimental information, and a crystallographic information file (CIF) of $Nd_{0.9}Sr_{0.1}BaInO_{3.95}$. See DOI: 10.1039/c5ta01336d

Open Access Article. Published on 20 April 2015. Downloaded on 7/22/2025 6:37:52 AM.
This article is licensed under a Creative Commons Attribution 3.0 Unported Licence.

Electrical conductivity measurements

The electrical conductivities of $Nd_{1-x}Sr_xBaInO_{4-x/2}$ ($x = 0.0$, 0.1, 0.2, and 0.3) were measured using a DC 4-probe method using sintered pellets (*ca.* 4.4 mm $\phi \times 30$ mm with densities in the range of 90–95% of theoretical density) with Pt electrodes over the temperature range from 400 °C to 1200 °C in air. The oxygen partial pressure $P(O_2)$ dependence of the electrical conductivities of $NdBaInO_4$ and $Nd_{0.9}Sr_{0.1}BaInO_{3.95}$ was measured at 858 °C using N_2/H_2, N_2/CO_2, and N_2/O_2 gas mixtures. The $P(O_2)$ was monitored by an oxygen sensor that was set close to the sample. The oxide-ion conductivities of $NdBaInO_4$ and $Nd_{0.9}Sr_{0.1}BaInO_{3.95}$ were measured from 610 °C to 1100 °C under $P(O_2) = 3.6 \pm 2.6 \times 10^{-17}$ atm for $NdBaInO_4$ and $P(O_2) = 8.8 \pm 6.2 \times 10^{-14}$ atm for $Nd_{0.9}Sr_{0.1}BaInO_{3.95}$.

Neutron and synchrotron X-ray diffraction measurements

Synchrotron X-ray powder diffraction (XRPD) measurements were conducted using a Debye–Scherrer camera with an imaging plate on beam line BL19B2 at SPring-8 (27 °C; wavelength = 0.399662(2) Å).[9] Room temperature time-of-flight (TOF) neutron powder diffraction (NPD) measurements (24 °C) were performed using the iMATERIA diffractometer of the J-PARC facility, Tokai, Japan.[10] High-temperature angle dispersive-type NPD measurements (800 °C using a vacuum furnace; wavelength = 1.83432(4) Å) were performed using a neutron powder diffractometer HRPD installed at HANARO reactor, KAERI, Korea.[11]

Results and discussion

XRPD patterns of $Nd_{1-x}Sr_xBaInO_{4-x/2}$ ($x = 0.0$, 0.1, 0.2, 0.3, and 0.4) identified the final products to be the monoclinic $P2_1/c$ $NdBaInO_4$ phase, except $x = 0.4$, which showed a different XRPD pattern with additional peaks, indicating possible saturation of the dopant within the $NdBaInO_4$ structure (Fig. 1a). We found that the total electrical conductivity of $Nd_{0.9}Sr_{0.1}BaInO_{3.95}$ is higher than that of $NdBaInO_4$, $Nd_{0.8}Sr_{0.2}BaInO_{3.9}$, and $Nd_{0.7}Sr_{0.3}BaInO_{3.85}$ (Fig. 1b). Therefore, we focused on the $Nd_{0.9}Sr_{0.1}BaInO_{3.95}$ composition for further detailed studies.

Fig. 2a shows the $P(O_2)$ dependence of the total electrical conductivity σ_{total} of $NdBaInO_4$ and $Nd_{0.9}Sr_{0.1}BaInO_{3.95}$ at 858 °C. With decreasing $P(O_2)$, the σ_{total} decreased in the high $P(O_2)$ range (region [A] and [B] in Fig. 2a), was constant in the intermediate $P(O_2)$ range (region [C] in Fig. 2a) and increased in the low $P(O_2)$ range (region [D] in Fig. 2a). The slope of $\log(\sigma_{total})$ versus $\log(P(O_2))$ of $NdBaInO_4$ in the $P(O_2)$ range from 5.9×10^{-4} to 2.0×10^{-1} atm is 0.215(2) and of $Nd_{0.9}Sr_{0.1}BaInO_{3.95}$ in the $P(O_2)$ range from 5.7×10^{-3} to 2.0×10^{-1} atm is 0.216(6), which indicates that these materials show p-type conductivity in region [A], and mixed oxide-ion and hole conduction in region [B]. The constant conductivities independent of $P(O_2)$ in region [C] indicate that both $NdBaInO_4$ and $Nd_{0.9}Sr_{0.1}BaInO_{3.95}$ materials show pure oxide-ion conduction.

Fig. 2b shows Arrhenius plots of the total electrical conductivity σ_{total} (circles in Fig. 2b) and oxide-ion conductivity σ_{ion} (triangles in Fig. 2b) of $NdBaInO_4$ (black) and $Nd_{0.9}Sr_{0.1}BaInO_{3.95}$ (red). Over the entire temperature range, the total electrical conductivity σ_{total} and oxide-ion conductivity σ_{ion} of $Nd_{0.9}Sr_{0.1}BaInO_{3.95}$ are higher than those of $NdBaInO_4$. For example, the σ_{total} and σ_{ion} of $Nd_{0.9}Sr_{0.1}BaInO_{3.95}$ at 858 °C were 7.3×10^{-3} S cm^{-1} and 7.7×10^{-4} S cm^{-1}, respectively, are higher than those of $NdBaInO_4$ 1.0×10^{-3} S cm^{-1} and 3.6×10^{-5} S cm^{-1}, respectively. The hole conductivities of $Nd_{0.9}Sr_{0.1}BaInO_{3.95}$ and $NdBaInO_4$ were calculated to be 6.5×10^{-3} and 9.6×10^{-4} S cm^{-1}, respectively, at 858 °C. The activation energies of total, oxide-ion, and hole conductivities of $Nd_{0.9}Sr_{0.1}BaInO_{3.95}$ were 0.685(7), 0.795(10), and 0.673 eV, which are lower than those of $NdBaInO_4$ (0.952(13), 0.91(4), and 0.953 eV). Therefore, 10 mol% Sr doping into $NdBaInO_4$ improves the oxide-ion conductivity and lowers its activation energy.

To investigate the structure changes in $NdBaInO_4$ by 10 mol% Sr doping, Rietveld analysis was conducted for $Nd_{0.9}Sr_{0.1}BaInO_{3.95}$ based on the synchrotron XRPD and NPD data using RIETAN-FP[12] and Z-Code.[13] $Nd_{0.9}Sr_{0.1}BaInO_{3.95}$ is isostructural with $NdBaInO_4$ (space group $P2_1/c$) and has seven

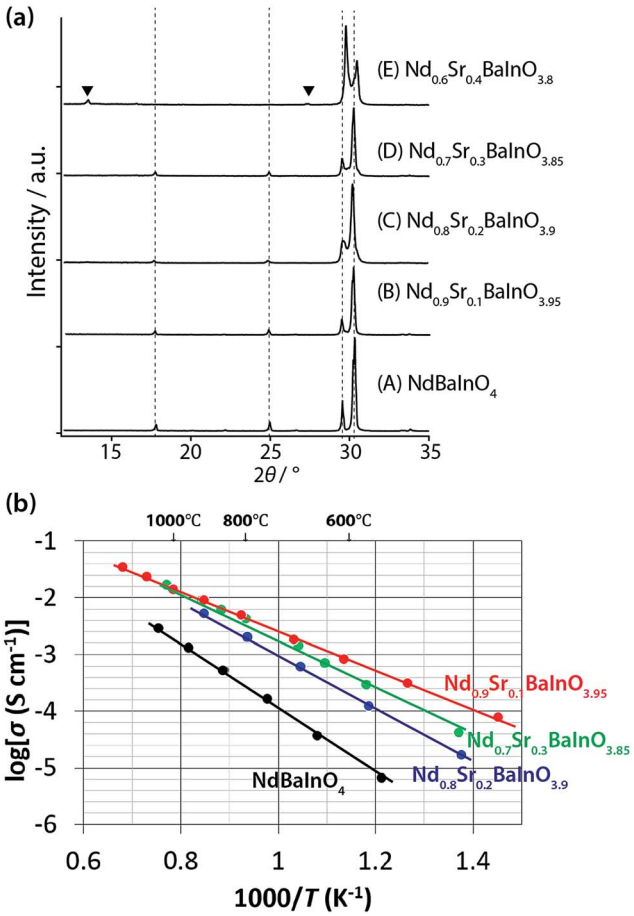

Fig. 1 (a) X-ray powder diffraction patterns of (A) $NdBaInO_4$, (B) $Nd_{0.9}Sr_{0.1}BaInO_{3.95}$, (C) $Nd_{0.8}Sr_{0.2}BaInO_{3.9}$, (D) $Nd_{0.7}Sr_{0.3}BaInO_{3.85}$, and (E) $Nd_{0.6}Sr_{0.4}BaInO_{3.8}$. The dashed lines indicate the peak positions of the pure $NdBaInO_4$ phase. The black triangles show additional peaks that only appeared in $Nd_{0.6}Sr_{0.4}BaInO_{3.8}$. (b) Total electrical conductivities of $NdBaInO_4$ (black), $Nd_{0.9}Sr_{0.1}BaInO_{3.95}$ (red), $Nd_{0.8}Sr_{0.2}BaInO_{3.9}$ (blue), and $Nd_{0.7}Sr_{0.3}BaInO_{3.85}$ (green) measured in air.

This journal is © The Royal Society of Chemistry 2015

Open Access Article. Published on 20 April 2015. Downloaded on 7/22/2025 6:37:52 AM.
This article is licensed under a Creative Commons Attribution 3.0 Unported Licence.

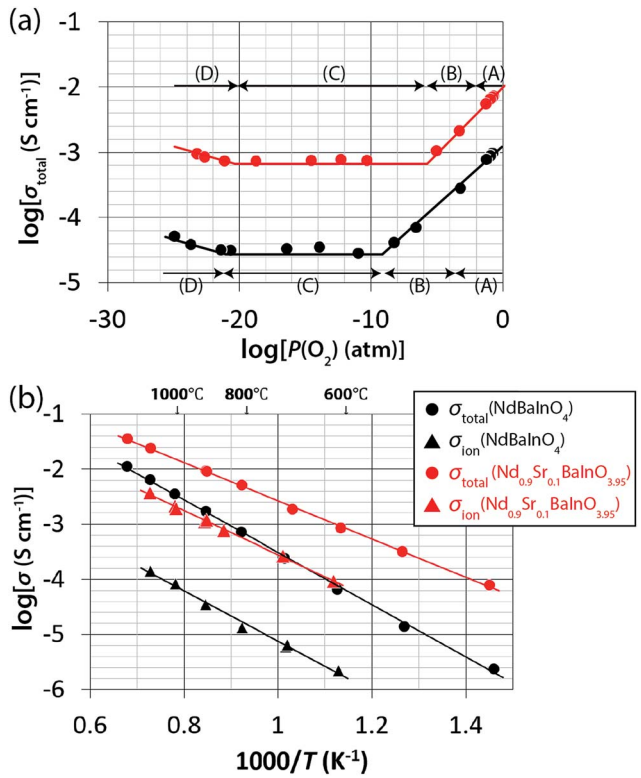

Fig. 2 (a) Partial oxygen pressure $P(O_2)$ dependence of the total electrical conductivity σ_{total} (858 °C) of $NdBaInO_4$ (black) and $Nd_{0.9}Sr_{0.1}BaInO_{3.95}$ (red). The dominant carriers are electron holes in $P(O_2)$ region [A], oxide ions and electron holes in [B], oxide ions in [C], and the oxide ions and electrons in [D]. (b) Arrhenius plots of the total conductivity σ_{total} (circles) and ionic conductivity σ_{ion} (triangles) of $NdBaInO_4$ (black) and $Nd_{0.9}Sr_{0.1}BaInO_{3.95}$ (red). σ_{total} values were measured in air and σ_{ion} values were measured under $P(O_2) = 3.6 \pm 2.6 \times 10^{-17}$ atm for $NdBaInO_4$ and $P(O_2) = 8.8 \pm 6.2 \times 10^{-14}$ atm for $Nd_{0.9}Sr_{0.1}BaInO_{3.95}$.

independent sites at the general position, Nd, Ba, In, O1, O2, O3, and O4 (Table 2).[8] The site preference of Sr was investigated in a preliminary analysis that gave the best reliable factors, R_{wp} and R_B, in the case that Sr exists at the Nd site (Table S2 in (ESI†)). Here, R_{wp} is the weighted reliability factor of profile intensity and R_B is the reliability factor based on integrated intensities. Therefore, the occupancy factors were fixed to $g(Nd,Nd) = 0.9$ and $g(Sr,Nd) = 0.1$ in the final refinement. Here, $g(Y,X)$ represents the occupancy factor of atom Y at the X site. The refinement of the occupancy factors of the oxygen atoms using common values for all oxygen atoms yields 0.9842(10), which clearly indicates the existence of oxygen vacancies. The value agrees with the expected value of 0.9875 calculated from the charge balance. In the final refinement, the occupancy factors of oxygen atoms were fixed to 0.9875. The TGA of $Nd_{0.9}Sr_{0.1}BaInO_{3.95}$ showed 0.18% weight loss between 50 and 800 °C, which corresponds to $\delta = 0.05$ of $Nd_{0.9}Sr_{0.1}BaInO_{3.95-\delta}$ (Fig. 3). Here, $(0.05 + \delta)$ is the amount of oxygen vacancies. Thus, the occupancy factors of oxygen atoms were fixed to 0.975 for the high-temperature (800 °C) data. The final Rietveld patterns are shown in Fig. 4a and b. The final refined atomic coordinates are shown in Table 1 for the TOF neutrons data and Table S1 in the ESI† for the synchrotron X-ray and the angle dispersive type neutron data.

Comparing the unit-cell parameters between 24 °C and 800 °C, the a-, b- and c-axes increased and the β-angle decreased with increasing temperature. The average thermal expansion coefficients between 24 °C and 800 °C were found to be $\alpha_a = 1.23(4) \times 10^{-5}\ K^{-1}$, $\alpha_b = 1.07(3) \times 10^{-5}\ K^{-1}$, $\alpha_c = 0.72(4) \times 10^{-5}\ K^{-1}$, $\alpha_\beta = -3.73(17) \times 10^{-5}\ K^{-1}$, and $\bar{\alpha} = 1.06(2) \times 10^{-5}\ K^{-1}$ (the definition of these coefficients are described in section D of the ESI†). These average thermal expansion coefficients of $Nd_{0.9}Sr_{0.1}BaInO_{3.95}$ are similar to those of $NdBaInO_4$ between 20 °C and 1000 °C ($\alpha_a = 1.42(2) \times 10^{-5}\ K^{-1}$, $\alpha_b = 1.176(14) \times 10^{-5}\ K^{-1}$, $\alpha_c = 0.77(3) \times 10^{-5}\ K^{-1}$, $\alpha_\beta = -3.81(4) \times 10^{-5}\ K^{-1}$,

Table 1 Crystallographic data of $Nd_{0.9}Sr_{0.1}BaInO_{3.95-\delta}$. Comparison with $NdBaInO_4$

Source and facility	TOF[a] Neutron iMATERIA, J-PARC	Synchrotron BL19B2, SPring-8	Neutron HRPD, HANARO	Ref. 8
Chemical formula	$Nd_{0.9}Sr_{0.1}BaInO_{3.95}$	$Nd_{0.9}Sr_{0.1}BaInO_{3.95}$	$Nd_{0.9}Sr_{0.1}BaInO_{3.90}$	$NdBaInO_{4.00}$
Formula weight	453.92	453.92	453.20	460.39
Temperature / °C	24	27	800	20
Wavelength / Å	Time of flight (d = 0.494–5.223 Å)	0.399662(2)	1.83432(4)	
Crystal system	Monoclinic	Monoclinic	Monoclinic	Monoclinic
Space group	$P2_1/c$	$P2_1/c$	$P2_1/c$	$P2_1/c$
a / Å	9.106468(17)	9.10285(12)	9.2060(17)	9.09538(3)
b / Å	6.050490(11)	6.04769(5)	6.0999(11)	6.04934(2)
c / Å	8.268786(19)	8.26670(9)	8.2984(17)	8.25620(2)
β / Å	103.40613(14)	103.3924(9)	103.057(12)	103.4041(3)
Unit-cell volume / Å^3	443.184(2)	442.716(8)	453.95(15)	441.89(2)
Z	4	4	4	4
Calculated density / Mg m^{-3}	6.81	6.81	6.64	6.92
R_{wp}	0.0458	0.0230	0.0362	
R_p	0.0334	0.0150	0.0280	—
Goodness of fit	2.994	1.000	1.860	—
R_B	0.0534	0.0139	0.0297	—
R_F	0.0295	0.0117	0.0156	—

[a] TOF: Time-of-Flight.

Open Access Article. Published on 20 April 2015. Downloaded on 7/22/2025 6:37:52 AM.
This article is licensed under a Creative Commons Attribution 3.0 Unported Licence.

Table 2 Occupancy factors, atomic coordinates and atomic displacement parameters of $Nd_{0.9}Sr_{0.1}BaInO_{3.95}$ obtained from the time-of-flight neutron powder diffraction data (iMATERIA, J-PARC) measured at 24 °C

Site label X	Atom Y	$g(Y,X)$[a]	x	y	z	U[b] (Å^2)
Nd	Nd	0.9	0.45269(5)	0.74731(11)	0.10734(6)	0.00819 (U_{eq})[c]
	Sr	0.1				
Ba	Ba	1	0.14825(7)	0.25034(18)	0.0328(11)	0.00933 (U_{eq})
In	In	1	0.83211(9)	0.2545(2)	0.20649(14)	0.0030(19)
O1	O	0.9875	0.18155(8)	0.80285(9)	0.04782(12)	0.01422 (U_{eq})
O2	O	0.9875	0.98669(11)	0.98872(17)	0.26951(12)	0.00988 (U_{eq})
O3	O	0.9875	0.38341(9)	0.5429(13)	0.32909(11)	0.01730 (U_{eq})
O4	O	0.9875	0.65046(8)	0.50812(15)	0.12937(11)	0.01549 (U_{eq})

Site label X	U_{11}[d] (Å^2)	U_{22} (Å^2)	U_{33} (Å^2)	U_{12} (Å^2)	U_{13} (Å^2)	U_{23} (Å^2)
Nd	0.0065(3)	0.0051(2)	0.0063(3)	0.0001(3)	−0.0008(2)	0.0020(3)
Ba	0.0078(3)	0.0018(3)	0.0106(4)	0.0010(5)	0.0032(3)	0.0019(5)
O1	0.0170 (4)	0.0148(5)	0.0094(3)	0.0055(4)	0.0064(3)	0.0077(5)
O2	0.0048(3)	0.0090(3)	0.0148(5)	0.0056(3)	−0.0000(3)	0.0048(5)
O3	0.01516(5)	0.0194(5)	0.0131(5)	0.0059(4)	0.0016(4)	0.0032(5)
O4	0.0091(4)	0.0142(5)	0.0220(5)	0.0060(4)	−0.0041(4)	−0.007(4)

[a] $g(Y,X)$: occupancy factor of atom Y at the X site. [b] Atomic displacement parameter. [c] Equivalent isotropic atomic displacement parameter. [d] U_{ij}: anisotropic atomic displacement parameter.

and $\bar{\alpha} = 1.176(15) \times 10^{-5}$ K^{-1}). There was an anisotropy observed in the thermal expansion. The average thermal expansion coefficients are similar for the *a*- and *b*-axes, whereas that of the *c*-axis is lower than the others. The average linear thermal expansion coefficients $\bar{\alpha}$ of $Nd_{0.9}Sr_{0.1}BaInO_{3.95}$ (1.06(2) $\times 10^{-5}$ K^{-1}) and $NdBaInO_4$ (1.176(15) $\times 10^{-5}$ K^{-1}) are close to that of yttria stabilized zirconia (YSZ), which is favourable for using this material as a cathode in SOFC applications. The average thermal expansion coefficients of 3 and 8 mol% Y_2O_3–ZrO_2 between 20 and 1000 °C were reported to be 1.08×10^{-5} and 1.05×10^{-5} K^{-1}, respectively.[14]

The crystal structure of $Nd_{0.9}Sr_{0.1}BaInO_{3.95}$ at 24 °C comprises the A rare earth structure A_2O_3 ($(Nd,Sr)_2O_3$) and the perovskite $(A,A')BO_3$ ($(Nd,Sr)_{2/8}Ba_{6/8}InO_3$) units (Fig. 4c) which belongs to the same structural family as $NdBaInO_4$.[8] Here, *A* and *A*′ are relatively large cations and *B* is a smaller cation. The unit-cell volume at 24 °C of $Nd_{0.9}Sr_{0.1}BaInO_{3.95}$ (443.184(2) Å^3) is slightly larger than that of $NdBaInO_4$ (441.8905(3) Å^3). The larger volume is ascribed to the larger ionic radius[15] of Sr^{2+} (1.21 Å for coordination number (CN) of 7) than that of Nd^{3+} (1.046 Å for CN = 7). The calculated bond valence sums (BVSs)[16] from the bond lengths are 1.77 for Ba, 2.85 for ($Nd_{0.9}Sr_{0.1}$) and 2.99 for In sites in $Nd_{0.9}Sr_{0.1}BaInO_{3.95}$. These values are consistent with their formal charges 2, 2.9, and 3, respectively, which indicates the validity of the refined crystal structure of $Nd_{0.9}Sr_{0.1}BaInO_{3.95}$.

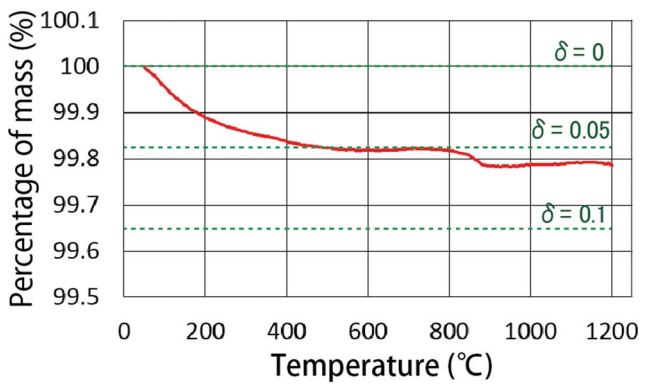

Fig. 3 TGA curve of $Nd_{0.9}Sr_{0.1}BaInO_{3.95-\delta}$ measured in Ar. This figure shows the second cycle (first and third cycles are shown in the ESI†). The green dash lines indicate the δ of $Nd_{0.9}Sr_{0.1}BaInO_{3.95-\delta}$. The weight loss from 50 to 800 °C was 0.18 wt%, which corresponds to the increase in the oxygen vacancy content $\delta = +0.05$.

As described above, $Nd_{0.9}Sr_{0.1}BaInO_{3.95}$ contains oxygen vacancies, while there are no significant oxygen vacancies within the 3σ of refined occupancy in $NdBaInO_4$ at room temperature, where σ is the estimated standard deviation.[8] Considering that $Nd_{0.9}Sr_{0.1}BaInO_{3.95}$ has a much higher oxide-ion conductivity than $NdBaInO_4$, the dominant carrier for the oxide-ion conduction in $Nd_{0.9}Sr_{0.1}BaInO_{3.95}$ is the oxygen vacancy. The activation energy of the oxide-ion conduction is a little lower for $Nd_{0.9}Sr_{0.1}BaInO_{3.95}$ (0.795(10) eV) than that for $NdBaInO_4$ (0.91(4) eV). The lower activation energy of $Nd_{0.9}Sr_{0.1}BaInO_{3.95}$ is attributable to the larger bottleneck size for the oxide-ion diffusion in $Nd_{0.9}Sr_{0.1}BaInO_{3.95}$ compared with $NdBaInO_4$. TGA of $NdBaInO_4$, and $Nd_{0.9}Sr_{0.1}BaInO_{3.95}$ showed little weight loss (around 0.02%) above 600 °C. Therefore, the effect of the carrier concentrations on the activation energy is thought to be negligible.

Diffusion pathways of oxide ions in the crystal structure of $Nd_{0.9}Sr_{0.1}BaInO_{3.95}$ and $NdBaInO_4$ were investigated by the bond valence based energy (BVE)[17] using the program

 This journal is © The Royal Society of Chemistry 2015

Open Access Article. Published on 20 April 2015. Downloaded on 7/22/2025 6:37:52 AM.
This article is licensed under a Creative Commons Attribution 3.0 Unported Licence.

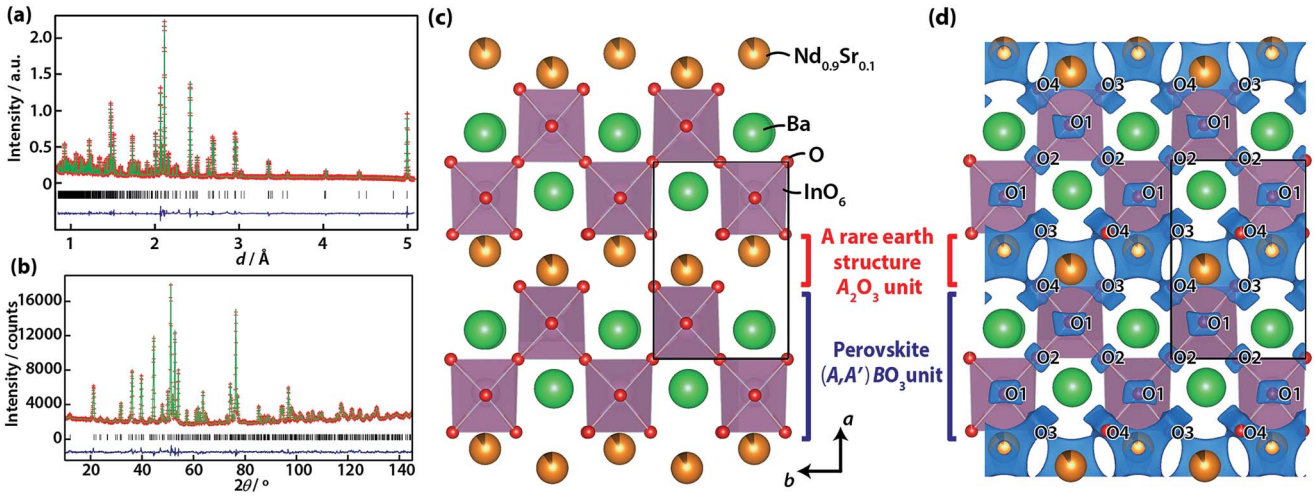

Fig. 4 Rietveld patterns for NPD data of (a) $Nd_{0.9}Sr_{0.1}BaInO_{3.95}$ taken at 24 °C (iMATERIA) and of (b) $Nd_{0.9}Sr_{0.1}BaInO_{3.90}$ at 800 °C (HRPD), showing the experimental (red + marks), calculated (green solid line) and difference (blue lower line) plots. Black tick marks indicate the calculated Bragg peak positions. (c) Refined crystal structure of $Nd_{0.9}Sr_{0.1}BaInO_{3.95}$ at 24 °C viewed along the *c*-axis. The solid lines represent the unit cell. (d) Bond valence-based energy (BVE) landscape for an oxide ion with an isovalue at 1.6 eV in $Nd_{0.9}Sr_{0.1}BaInO_{3.90}$ at 800 °C. Here, *A* and *A*′ are relatively large cations ((Nd,Sr) and Ba in this case) and *B* is a smaller cation (In in this case).

3DBVSMAPPER[18] based on the crystal structure at 800 °C. The blue surfaces in Fig. 4d represent the isosurfaces where the BVE for an oxide ion is +1.6 eV. In this landscape, the most stable position (at O4) was set to 0 eV. BVE isosurfaces around O1 and O2 sites are localized, while those around O3 and O4 sites spread in the A rare earth structure A_2O_3 ($(Nd,Sr)_2O_3$) unit and are connected with each other along both the *b*- and *c*-axes. The lowest energy path for oxide-ion conduction in $Nd_{0.9}Sr_{0.1}BaInO_{3.95}$ was found to be along the *b*-axis with an energy barrier of 1.42 eV. The energy barriers of the path along the *a*- and *c*-axes were calculated to be 2.72 and 1.47 eV for $Nd_{0.9}Sr_{0.1}BaInO_{3.95}$. The paths along the *b*- and *c*-axes have similar energy barriers and the path along the *a*-axis has significantly higher energy barriers than the others. Thus, the oxide-ion conduction in $Nd_{0.9}Sr_{0.1}BaInO_{3.95}$ would be two dimensional.

BVE barriers of $Nd_{0.9}Sr_{0.1}BaInO_{3.95}$ have lower values than those of $NdBaInO_4$ along the oxide-ion diffusion paths. The energy barriers along the *a*-, *b*- and *c*-axes calculated based on the crystal structures at 24 °C are 1.47, 2.88, and 1.69 eV for $Nd_{0.9}Sr_{0.1}BaInO_{3.95}$ and 1.72, 3.95, and 2.01 for $NdBaInO_4$. These results are consistent with the experimental data that showed that $Nd_{0.9}Sr_{0.1}BaInO_{3.95}$ has a lower activation energy of oxide-ion diffusion than $NdBaInO_4$. The highest BVE point along the possible oxide-ion diffusion path is surrounded by two (Nd or (Nd,Sr)) and one Ba cations, which forms a cation triangle bottleneck. The areas of the triangles were calculated to be 6.889(5) Å^2 for $NdBaInO_4$ and 6.911(3) Å^2 for $Nd_{0.9}Sr_{0.1}BaInO_{3.95}$. Thus, the substitution of Nd with Sr increases this bottleneck area, and hence, lowers the activation energy of oxide-ion conduction.

Conclusions

The oxide-ion conductivity has been increased and the activation energy of oxide-ion conduction has been lowered by the substitution of Nd with Sr cations in $NdBaInO_4$. $Nd_{0.9}Sr_{0.1}BaInO_{3.95}$ showed the highest electrical conductivity among $Nd_{1-x}Sr_xBaInO_{4-x/2}$ (x = 0.0, 0.1, 0.2 and 0.3). The oxide-ion conductivity σ_{ion} of $Nd_{0.9}Sr_{0.1}BaInO_{3.95}$ was 7.7×10^{-4} S cm^{-1} at 858 °C, which is higher than that of $NdBaInO_4$ ($\sigma_{ion} = 3.6 \times 10^{-5}$ S cm^{-1} at 858 °C). The crystal structure of $Nd_{0.9}Sr_{0.1}BaInO_{3.95}$ has been analysed, and we have confirmed that Sr exists at the Nd site. $Nd_{0.9}Sr_{0.1}BaInO_{3.95}$ contains oxygen vacancies, which were not observed for $NdBaInO_4$ at room temperature. Thus, the increase of the oxide-ion conductivity is mainly attributed to the increase of the carrier concentration. BVE calculations indicated two-dimensional oxide-ion diffusion in the A_2O_3 ($(Nd,Sr)_2O_3$) unit on the *bc*-plane and a decrease of the energy barrier by the substitution of Nd with Sr cations.

Acknowledgements

We thank Dr K. Osaka for assistance with the synchrotron diffraction experiments and Prof. T. Ishigaki for assistance with the neutron diffraction experiments. The synchrotron radiation experiments were conducted on BL19B2 at SPring-8 (Proposal no. 2013B1718, 2014A1510, 2014B1660, and 2014B1922) and on BL-4B2 of the Photon Factory (Proposal no. 2013G216, 2013G053, and 2014G508). The neutron-diffraction experiments were conducted on the diffractometer iMATERIA at J-PARC (Proposal no. 2013A0136, 2013B0178, 2014A0011, and 2014B0114) and on the diffractometer HRPD at HANARO (Proposal no. NB-HRPD/2013-000026, 27, 2014-0071, and 72). We thank the Center for Materials Analysis at O-okayama of Tokyo Institute of Technology for the ICP-OES measurements. This study was partially supported by a Grant-in-Aid for Scientific Research (KAKENHI, no. 24850009, 24246107, 24226016, 25630365, 15H02291) from the Ministry of Education, Culture, Sports, Science and Technology of Japan and by the Murata Science Foundation. Neutron experiments at HANARO were

partially supported by the National Research Foundation of Korea under Contract NRF-2012M2A2A6004261. Travel cost for HANARO neutron experiments was partially supported by the Institute for Solid State Physics, The University of Tokyo (proposal no. 12725, 13679, 14643 and 14657), Japan Atomic Energy Agency, Tokai, Japan.

Open Access Article. Published on 20 April 2015. Downloaded on 7/22/2025 6:37:52 AM.
This article is licensed under a Creative Commons Attribution 3.0 Unported Licence.

Notes and references

1 (*a*) J. B. Goodenough, *Nature*, 2000, **404**, 821; (*b*) J. B. Goodenough, *Annu. Rev. Mater. Res.*, 2003, **33**, 91; (*c*) V. Thangadurai and W. Weppner, *Ionics*, 2006, **12**, 81; (*d*) D. J. L. Brett, A. Atkinson, N. P. Brandon and S. J. Skinner, *Chem. Soc. Rev.*, 2008, **37**, 1568; (*e*) L. Malavasi, C. A. J. Fisher and M. S. Islam, *Chem. Soc. Rev.*, 2010, **39**, 4370; (*f*) S. Y. Istomin and E. V. Antipov, *Russ. Chem. Rev.*, 2013, **82**, 686; (*g*) A. B. Muñoz-García, A. M. Ritzmann, M. Pavone, J. A. Keith and E. A. Carter, *Acc. Chem. Res.*, 2014, **47**, 3340.

2 (*a*) J. C. Boivin and G. Mairesse, *Chem. Mater.*, 1998, **10**, 2870; (*b*) J. A. Kilner and M. Burriel, *Annu. Rev. Mater. Res.*, 2014, **44**, 365.

3 (*a*) M. Mogensen, D. Lybye, N. Bonanos, P. V. Hendriksen and F. W. Poulsen, *Solid State Ionics*, 2004, **174**, 279; (*b*) M. Yashima, *Solid State Ionics*, 2008, **179**, 797.

4 (*a*) A. S. Bhalla, R. Guo and R. Roy, *Mater. Res. Innovations*, 2000, **4**, 3; (*b*) R. E. Schaak and T. E. Mallouk, *Chem. Mater.*, 2002, **14**, 1455; (*c*) S. Stølen, E. Bakken and C. E. Mohn, *Phys. Chem. Chem. Phys.*, 2006, **8**, 428; (*d*) M. Yashima, *J. Ceram. Soc. Jpn.*, 2009, **117**, 1055.

5 (*a*) V. V. Kharton, A. P. Viskup, E. N. Naumovkh and F. M. B. Marques, *J. Mater. Chem.*, 1999, **9**, 2623; (*b*) S. Miyoshi, T. Furuno, O. Sangoanruang, H. Matsumoto and T. Ishihara, *J. Electrochem. Soc.*, 2007, **154**, B57; (*c*) T. Ishihara, K. Nakashima, S. Okada, M. Enoki and H. Matsumoto, *Solid State Ionics*, 2008, **179**, 1367; (*d*) M. Yashima, M. Enoki, T. Wakita, R. Ali, Y. Matsushuta, F. Izumi and T. Ishihara, *J. Am. Chem. Soc.*, 2008, **130**, 2762; (*e*) M. Yashima, N. Sirikanda and T. Ishihara, *J. Am. Chem. Soc.*, 2010, **132**, 2379; (*f*) M. Yashima, H. Yamada, S. Nuansaeng and T. Ishihara, *Chem. Mater.*, 2012, **24**, 4100; (*g*) K. Kawamura, M. Yashima, K. Fujii, K. Omoto, K. Hibino, S. Yamada, J. R. Hester, M. Avdeev, P. Miao, S. Torii and T. Kamiyama, *Inorg. Chem.*, 2015, **54**, 3896.

6 X. Kuang, M. A. Green, H. Niu, P. Zajdel, C. Dicknson, J. B. Claridge, L. Jantsky and M. J. Rosseinsky, *Nat. Mater.*, 2008, **7**, 498.

7 (*a*) S. Nakayama and M. Sakamoto, *J. Eur. Ceram. Soc.*, 1998, **18**, 1413; (*b*) M. Higuchi, Y. Masubuchi, S. Nakayama, S. Kikkawa and K. Kodaira, *Solid State Ionics*, 2004, **174**, 73; (*c*) R. Ali, M. Yashima, Y. Matsushita, H. Yoshioka, K. Ohoyama and F. Izumi, *Chem. Mater.*, 2008, **20**, 5203.

8 K. Fujii, Y. Esaki, K. Omoto, M. Yashima, A. Hoshikawa, T. Ishigaki and J. R. Hester, *Chem. Mater.*, 2014, **26**, 2488.

9 http://www.spring8.or.jp/wkg/BL19B2/instrument/lang-en/INS-0000000300/instrument_summary_view.

10 T. Ishigaki, A. Hoshikawa, M. Yonemura, T. Morishima, T. Kamiyama, R. Oishi, T. Sakuma, Y. Tomota, M. Arai, M. Hayashi, K. Ebata, Y. Takano, H. Asano, Y. Takano and T. Kasao, *Nucl. Instrum. Methods Phys. Res., Sect. A*, 2009, **600**, 189.

11 http://hanaro.kaeri.re.kr:444/NB/sub02/sub02.do.

12 F. Izumi and K. Momma, *Solid State Phenom.*, 2007, **130**, 15.

13 (*a*) R. Oishi, M. Yonemura, Y. Nishimaki, S. Torii, A. Hoshikawa, T. Ishigaki, T. Morishima, K. Mori and T. Kamiyama, *Nucl. Instrum. Methods Phys. Res., Sect. A*, 2009, **600**, 94; (*b*) R. Oishi-Tomiyasu, M. Yonemura, T. Morishima, A. Hoshikawa, S. Torii, T. Ishigaki and T. Kamiyama, *J. Appl. Crystallogr.*, 2012, **45**, 299.

14 I. Yasuda and M. Hishinuma, *Electrochemistry*, 2000, **68**, 526.

15 R. D. Shannon, *Acta Crystallogr., Sect. A: Cryst. Phys., Diffr., Theor. Gen. Crystallogr.*, 1976, **32**, 751.

16 R. E. Brese and M. O'Keeffe, *Acta Crystallogr., Sect. B: Struct. Sci.*, 1991, **47**, 192.

17 (*a*) S. Adams, *Solid State Ionics*, 2000, **136**, 1351; (*b*) S. Adams, *Struct. Bonding*, 2014, **158**, 91; (*c*) M. Avdeev, M. Sale, S. Adams and R. P. Rao, *Solid State Ionics*, 2011, **225**, 43.

18 (*a*) M. Sale and M. Avdeev, *J. Appl. Crystallogr.*, 2012, **45**, 1054; (*b*) M. Yashima, N. Kubo, K. Omoto, H. Fujimori, K. Fujii and K. Ohoyama, *J. Phys. Chem. C*, 2014, **118**, 5180; (*c*) M. Yashima, T. Sekikawa, D. Sato, H. Nakano and K. Omoto, *Cryst. Growth Des.*, 2013, **13**, 829; (*d*) M. Yashima, Invited Review: Some recent developments in the atomic-scale characterization of structural and transport properties of ceria-based catalysts and ionic conductors, *Catal. Today*, 2015, DOI: 10.1016/j.cattod.2015.03.034, in press.

 This journal is © The Royal Society of Chemistry 2015